RESEARCH ARTICLE

The Elastic Behaviour of Sintered Metallic Fibre Networks: A Finite Element Study by Beam Theory

Wolfram A. Bosbach*

Engineering Department, University of Cambridge, Cambridge, United Kingdom

* wb248@cam.ac.uk

Abstract

Background

The finite element method has complimented research in the field of network mechanics in the past years in numerous studies about various materials. Numerical predictions and the planning efficiency of experimental procedures are two of the motivational aspects for these numerical studies. The widespread availability of high performance computing facilities has been the enabler for the simulation of sufficiently large systems.

Objectives and Motivation

In the present study, finite element models were built for sintered, metallic fibre networks and validated by previously published experimental stiffness measurements. The validated models were the basis for predictions about so far unknown properties.

Materials and Methods

The finite element models were built by transferring previously published skeletons of fibre networks into finite element models. Beam theory was applied as simplification method.

Results and Conclusions

The obtained material stiffness isn't a constant but rather a function of variables such as sample size and boundary conditions. Beam theory offers an efficient finite element method for the simulated fibre networks. The experimental results can be approximated by the simulated systems. Two worthwhile aspects for future work will be the influence of size and shape and the mechanical interaction with matrix materials.

Introduction

Background

The mechanics of metallic [1] and non-metallic [2] fibre networks have since long been the subject of research studies. One possible way to categorize the available studies is by the specific material which is investigated. Early and recent studies about cellulose material and paper can be found in [2–6]. Numerous studies exist about the mechanics of polymeric networks [7–11]. The modelling of polymeric non-woven fabrics and their particularly complex behaviour [12] has been in the focus of several research studies [13–17]. In the field of biomaterials, a big number of studies exists about the mechanics of actin networks and cytoskeletons [18–22]. A range of studies refers to theoretical networks whose geometries have been generated by computer code [23–31].

The mechanics of sintered, metallic fibre networks as used for the present study have been investigated by [1, 30–35]. In [36], an architectural characterization of the six network samples of the present study was published, together with experimentally obtained mechanical properties.

For finite element (FE) analyses of structures whose dimensions are dominated by their extension along only one axis, such as screws or fibres, beam theory can offer an efficient simulation method [37]. The foundations of beam theory were laid in [38–40] and are available in today's textbooks [41]. For the application of boundary conditions (BC) to random fibre networks and for the determination of the representative volume element (RVE), [29, 42] have provided a much referred to concept [43–46]. By this concept, the RVE is obtained for a defined relative error for each physical property. Image acquisition by computed tomography (CT) scanning which uses the principle of Röntgen radiation [47] is a commonly used method for measuring the dimensions of metallic three-dimensional (3D) structures [48].

Motivation and scope of the present study

The motivation of the present study was to predict previously unknown mechanical properties for metallic, sintered fibre networks. For that purpose, FE models were developed. The input geometries for the FE models were based on CT scans, acquired from real network samples in [36]. Experimental values for the network Young's modulus from that same study were used for a validation of the FE models. The properties of these six network samples define the scope and at the same time also the limitations of the present study. Other metallic, sintered networks with similar but different properties will require a re-evaluation of the proposed FE models.

Mathematical notation

Throughout the present study, the following notation is used: x for scalars, $\underline{x}$ for vectors, and $\underline{\underline{x}}$ for 2nd rank tensors. Cube faces are written X. The vector product is given as "×" and dot product as "·". Relations which are greater-than and approximately equal are written "$\gtrsim$". If the relation is greater-than or equal "$\geq$" is used.

Materials and Methods

Network samples and meshing step

The present study uses as geometry input for the FE models the dimensions of six AISI (American Iron and Steel Institute) 316L network samples. The architectural network values have been published in [36] (see Table 1). Each scanned sample section is a cube of volume $V = 4^3$ mm^3 (see Fig 1a). Following the two-phase model in [29], V is split into fibre volume and void

Table 1. AISI 316L network samples.

Sample	Fibre vol. frac. f [%]	Fibres [-]	Fibre segments [-]	Segment length λ [μm]	Beam elements [-]
316L-10%-No.1	10	2,891	22,913	235	700,515
316L-10%-No.2	10	2,815	22,789	239	709,427
316L-15%-No.1	15	4,326	37,049	191	929,249
316L-15%-No.2	15	4,920	41,479	181	1,029,453
316L-20%-No.1	20	6,138	59,936	153	1,265,910
316L-20%-No.2	20	6,400	59,949	153	1,269,925

Complete documentation of geometries in [36].
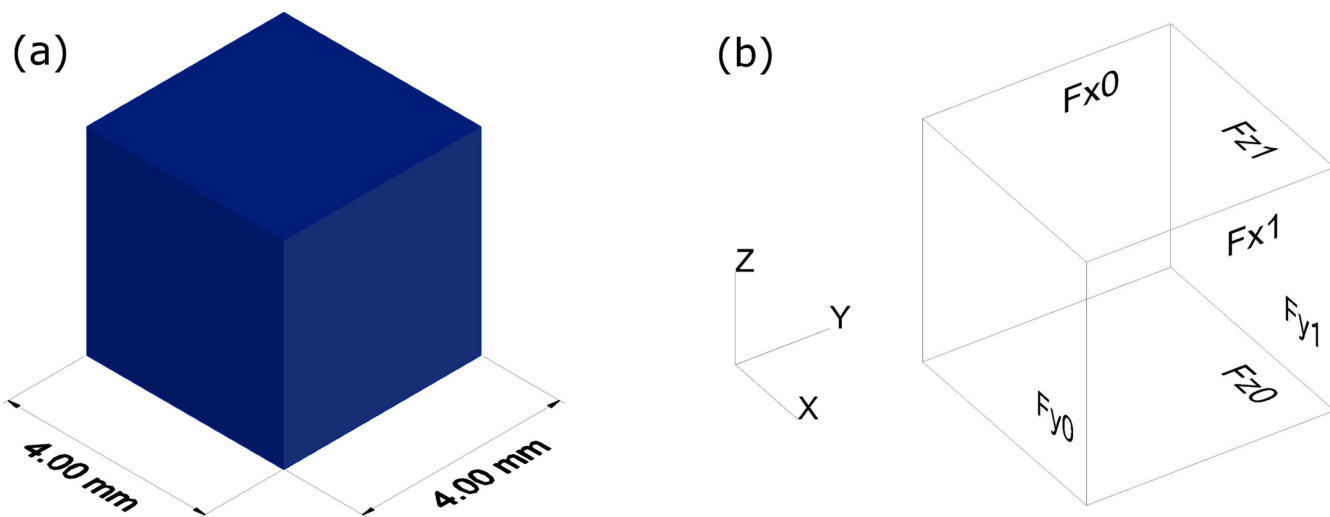
doi:10.1371/journal.pone.0143011.t001

Fig 1. Sample cube dimensions and definition of cube faces. (a) Dimensions of fibre network cube $V = 4^3$ mm^3 (fibre network details in [36]) and (b) six quadratic cube faces (F_{x0}, F_{x1}, F_{y0}, F_{y1}, F_{z0}, and F_{z1}) forming S.

doi:10.1371/journal.pone.0143011.g001

volume:

$$V = V_{fibre} \cup V_{void} \tag{1}$$

Equally, the volume boundary ∂V is defined to consist of a section of fibre boundary and a section of void boundary on the cube surface S:

$$\partial V = \partial V_{fibre} \cup \partial V_{void} \tag{2}$$

Six quadratic cube faces form S (see Fig 1b), two of them perpendicular each to one of the three axes:

$$S = F_{x0} \cup F_{y0} \cup F_{z0} \cup F_{x1} \cup F_{y1} \cup F_{z1} \tag{3}$$
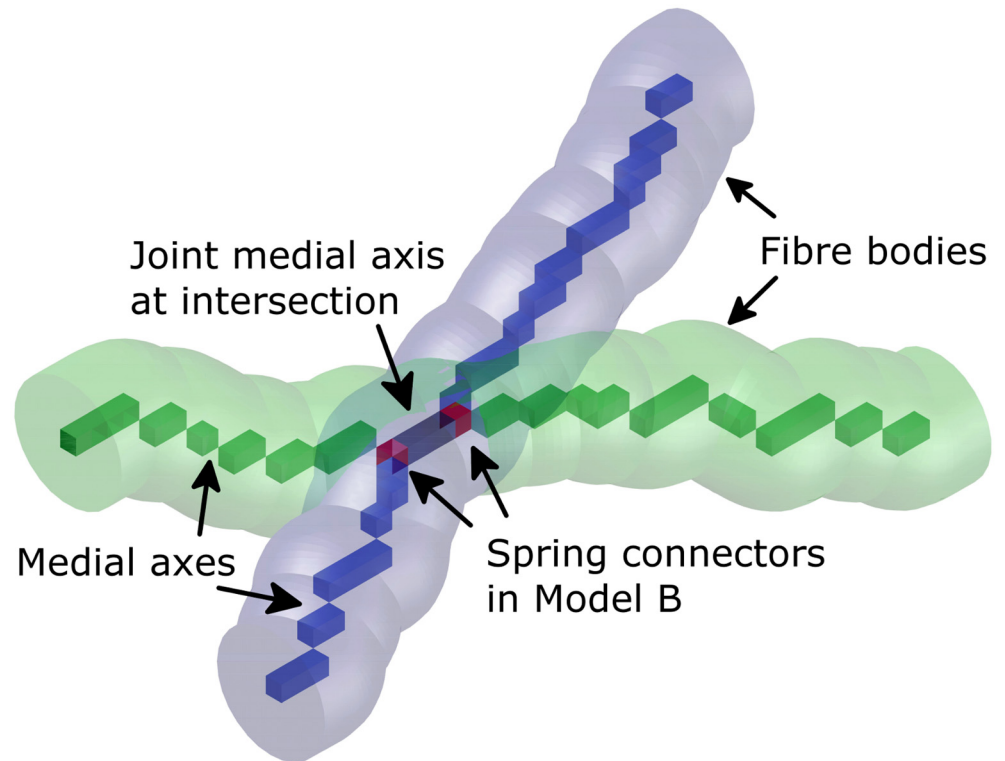
Fig 2. Medial axis model. Sketch of two intersecting fibre bodies with corresponding medial axes (green and blue) and joint medial axis at intersection (black) obtained by skeletonisation algorithm [50–52] in [36] and positions of spring connectors in Model B of the present study (red).

Two samples each are manufactured with a fibre volume fraction f of 10, 15, and 20%. In [36], the fibre production process by bundle drawing [49], the network manufacturing at N.V. Bekaert S.A. (Belgium), the CT scan acquisition at General Electric (resolution 7.75 μm), and the applied skeletonisation algorithm [50–52] are discussed in detail. The skeletonisation algorithm reduces the 3D fibre bodies to their medial axes which are strings of voxels (see Fig 2). The medial axis models obtained for [36] are transferred in the present study into beam assemblies and run as FE models. The approximately hexagonal fibre cross-section is simulated as a round cross-section of radius $R = 20$ μm.

FE models

For the present study, two FE models are implemented (see Table 2). Model A and Model B are based on five specifications:

1. Linear elasticity and static equilibrium,

2. Euler-Bernoulli or Timoshenko beam elements as AISI 316L fibres,

3. Rigid joints or torsional springs as inter-fibre joint models at contact points between fibre paths (see Fig 2),

4. BC as defined in Eqs (8) and (11), and

5. the new introduced model parameter of BC-depth h_{BC}.

Table 2. FE models.

	Joint model	Scaling factor	Beam element	BC-type	BC-depth
Model A	Rigid joint	*- not applicable -*	B31, B32, B33	KUBC, MBC	$0\ \mu m \leq h_{BC} \leq 155.00\ \mu m$
Model B	Spring joint	$s \in \{5, 10, 30, 300, 3000\}\ \mu m$	B31, B32	KUBC, MBC	$h_{BC} = 77.50\ \mu m = const$

doi:10.1371/journal.pone.0143011.t002

Linear elasticity and static equilibrium conditions. For mechanical FE analyses, the simulated system is transferred into a representation by the global stiffness matrix $\underline{K}$; the most common assembly method being the *direct stiffness method* [53]. $\underline{K}$ links the global load vector $\underline{F}$ and the global displacement vector $\underline{u}$:

$$\underline{F} = \underline{K} \cdot \underline{u} \qquad (4)$$

The meshed geometries and material specifications define the variables of $\underline{K}$. In the present study, the material is assumed to behave linearly elastic (i.e. fulfil Hook's law that stress and strain are linked by the Young's modulus: $\sigma = E\epsilon$ [54]). In this case, the variables of $\underline{K}$ become constants. The AISI 316L material stiffness is simulated as $E_{fibre} = 200\text{GPa}$ with a Poisson's ratio $v = 0.3$ which expresses the material's lateral contraction as fraction of the axial extension. For plastic or non-elastic simulations, the variables of $\underline{K}$ are functions of e.g. force or displacement.

BC are imposed in FE by prescribed values for entries of $\underline{F}$ and $\underline{u}$. The non-prescribed entries of $\underline{F}$ and $\underline{u}$ are determined by the FE solver (present study: Abaqus 6.13 [55]) with solutions respecting the equilibrium conditions of forces in Eq (5) and of moments in Eq (6) [56]. Both equations adopt the Lagrangian reference frame [57]. (A comparison to the Eulerian reference frame and its advantages for the modelling of fluids is available in [58].)

$$\int_{S} \underline{t}\ dS + \int_{V} \underline{f}\ dV = 0 \quad (\text{with } \underline{t} = \underline{\sigma} \cdot \underline{n}^{out}) \qquad (5)$$

$$\int_{S} (\underline{x} \times \underline{t})\ dS + \int_{V} (\underline{x} \times \underline{f})\ dV = 0 \qquad (6)$$

The surface traction vector $\underline{t}$ is obtained as the product of the Cauchy stress tensor $\underline{\sigma}$ and the unit outward normal $\underline{n}^{out}$. (A detailed discussion of $\underline{\sigma}$ is available in today's textbooks [59].) In the mechanical simulations of the present study, body force per volume $\underline{f}$ is neglected; gravitational forces or magnetic forces being typical examples for $\underline{f}$. The point vector $\underline{x}$ specifies the location of a point relative to the origin; i.e. also the equilibrium of moments in Eq (6) being taken about the origin.

Beam elements. One Euler-Bernoulli beam element (B33) and two Timoshenko beam elements, one with linear interpolation (B31) and one with quadratic interpolation (B32), are implemented for the present study. Table 3 contains the complete list of implemented Abaqus elements. The neglected shear strain of the Euler-Bernoulli beam and the advanced Timoshenko beam are further discussed in [41] for the simplified 2D case. Literature recommends in general for beam assemblies which include short beam elements the Timoshenko beam [28, 60–62]. For this case, [62] has documented an overestimation of the structural stiffness by Euler-Bernoulli beam elements.

Table 3. Implemented Abaqus elements.

Element Type	Abaqus identifier	Interpolation/Connection
Timoshenko Beam	B31	3D Linear
	B32	3D Quadratic
Euler-Bernoulli Beam	B33	3D Cubic
Spring connector	CONN3D2	3D Join & torsional spring

Complete software documentation in [55].

Inter-fibre joint models. Model A is simulated for rigid inter-fibre joints. Torsional spring elements (CONN3D2) are inserted into the medial axis models in Model B between intersecting fibre paths (see Fig 2). This concept for adaptive joint strength of Model B is proposed for comparable cases in publications such as [63]. In the present study, the inter-fibre joint stiffness K_{joint} is defined:

$$K_{joint} = sE_{fibre}A_{fibre} \tag{7}$$

The scaling factor s [m] in Eq (7) allows the directed variation of K_{joint} for an approximation of the experimental values of [36]. The cross-sectional area A_{fibre} and E_{fibre} are included as they relate the modelled value of K_{joint} to the fibre dimensions and to the fibre stiffness. Alternative model variables could be chosen too.

Kinematic uniform BC and load cases. In [42], a simulation set of kinematic uniform BC (KUBC), static uniform BC (SUBC), and periodic BC (PBC) was proposed for a random heterogeneous composite. KUBC are applied in the present study as defined in Eq (8). In the case of KUBC, a macroscopic strain tensor $\underline{\underline{E}}$ imposes the displacement vector $\underline{u}$ on all $\underline{x}$ located on ∂V:

$$\underline{u} = \underline{\underline{E}} \cdot \underline{x} \quad \forall \underline{x} \in \partial V \tag{8}$$

Six independent load cases are implemented in the present study by KUBC for the network samples: $i = 1$ to 3 for the simulation of tensile tests along the axes x, y, z and $i = 4$ to 6 for the corresponding shear tests. The combination of all six load cases leads to the symmetrical stiffness matrix $\underline{\underline{C}}$, where the six entries C_{ii} on the main diagonal stand for the Young's moduli E and Shear moduli G [64, 65]:

$$\begin{Bmatrix} \sigma_x \\ \sigma_y \\ \sigma_z \\ \tau_{yz} \\ \tau_{zx} \\ \tau_{xy} \end{Bmatrix} = \begin{bmatrix} C_{11} & C_{12} & C_{13} & C_{14} & C_{15} & C_{16} \\ \bullet & C_{22} & C_{23} & C_{24} & C_{25} & C_{26} \\ \bullet & \bullet & C_{33} & C_{34} & C_{35} & C_{36} \\ \bullet & \bullet & \bullet & C_{44} & C_{45} & C_{46} \\ \bullet & \bullet & \bullet & \bullet & C_{55} & C_{56} \\ \bullet & \bullet & \bullet & \bullet & \bullet & C_{66} \end{bmatrix} \begin{Bmatrix} \epsilon_x \\ \epsilon_y \\ \epsilon_z \\ \gamma_{yz} \\ \gamma_{zx} \\ \gamma_{xy} \end{Bmatrix} \tag{9}$$

$$\text{with}: \quad C_{11} = E_x, C_{22} = E_y, C_{33} = E_z$$
$$C_{44} = G_{yz}, C_{55} = G_{zx}, C_{66} = G_{xy}$$

The general 4th rank stiffness tensor contains in total 81 components. The simplification to only 21 independent variables in $\underline{C}$ is achieved by energy considerations and symmetry [66].

Mixed BC. The application of further BC to random fibre networks requires additional considerations [29]. In the case of SUBC, a macroscopic traction vector $\underline{\Gamma}$ is imposed on ∂V. PBC add a periodic fluctuation term $\underline{v}$. In [29], it is discussed for random fibre networks that considering:

$$\underline{\sigma} = 0 \ \forall \underline{x} \in V_{void} \tag{10}$$

$\underline{\Gamma}$ can't be prescribed on ∂V_{void}, only on ∂V_{fibre}. Due to the randomness of the fibre network geometry, the equilibrium conditions in Eqs (5) and (6) are not fulfilled when $\underline{\Gamma}$ is imposed. For overcoming this, mixed BC (MBC) are proposed by [29] and adopted in the present study for the simulation of tensile testing along the axes x and y by one independent load case each (load case $i = 1$ and 2, definition see above). A macroscopic strain tensor $\underline{\underline{E}}^{prim}$ imposes the primary displacement $\underline{u}^{prim}$ along the axis of tension only:

$$\underline{u}^{prim} = \underline{\underline{E}}^{prim} \cdot \underline{x} \ \ \forall \underline{x} \in \begin{cases} F_{x0} \cup F_{x1}, \text{ for } i = 1 \ (\text{tensile} - \text{x}) \\ \\ F_{y0} \cup F_{y1}, \text{ for } i = 2 \ (\text{tensile} - \text{y}) \end{cases} \tag{11}$$

Along the two non-prescribed axes, a secondary displacement $\underline{u}^{sec}$ is caused as a consequence of the imposed $\underline{u}^{prim}$. The total deformation of the sample is obtained under MBC as: $\underline{u}^{total} = \underline{u}^{prim} + \underline{u}^{sec}$.

The results obtained in [29] for the elastic modulus of computer generated random fibre networks without preferred orientation direction predict greater stiffness for KUBC: $C_{\text{MBC}} < C_{\text{KUBC}}$.

BC-depth. The present study extends the BC model of Eqs (8) and (11) for the investigated material by the variable of h_{BC}. The value of h_{BC} prescribes to which depth into the material along the inward normal $\underline{n}^{in}$ BC are imposed on ∂V. The reason for the model modification is the obtained structural response which will be discussed further in the following section by Model A in Figs 3 and 4.

Representative volume element determination

For the determination of the RVE size V_{RVE}, the present study relied on an algorithm proposed by [42]. This algorithm has been applied since its publication to random fibre networks in [29, 32] and other materials [43–46].

In [42], V_{RVE} is obtained as a probability estimate. The RVE is understood as the minimum cube volume V_{RVE} for which a particular physical property Z after n realisations can be determined within the margin of the relative error ϵ_{rel}. Due to this definition, V_{RVE} is in each case a function of these three variables (see Eq (20)).

In order to acquire the input for the RVE algorithm, the available material sample is split into sets of sub-samples of V_k (with $L_k = V_k^{1/3}$) of n_k realisations. The size function of the RVE is then determined by a regression analysis for the standard deviation $D_{Z(V_k)}$ of Z over V_k. In [45], the mean for V_k of a physical property $Z_{(V_k)}$ and the respective variation $D_{Z(V_k)}^2$ are
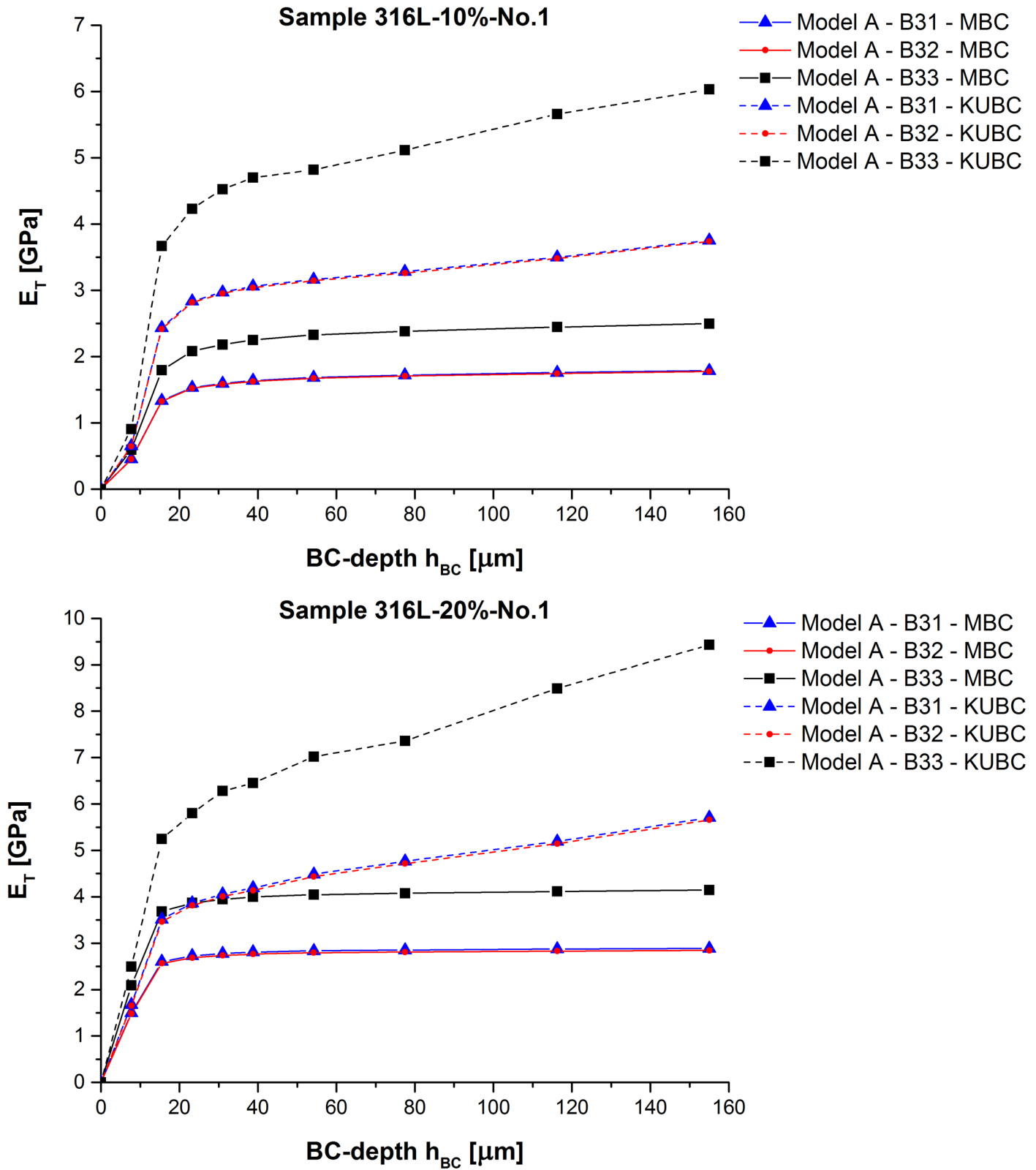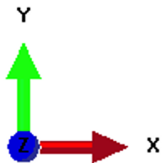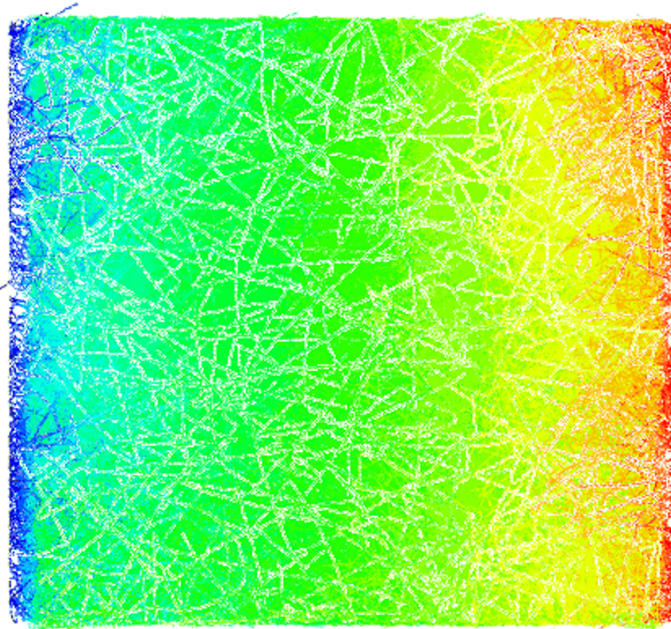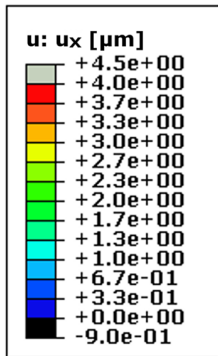
Fig 3. **Model A—Influence of BC-depth.** Obtained E_T values of samples 316L-10%-No.1, and 316L-20%-No.1 depending on h_{BC}.
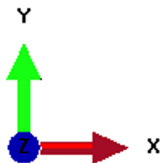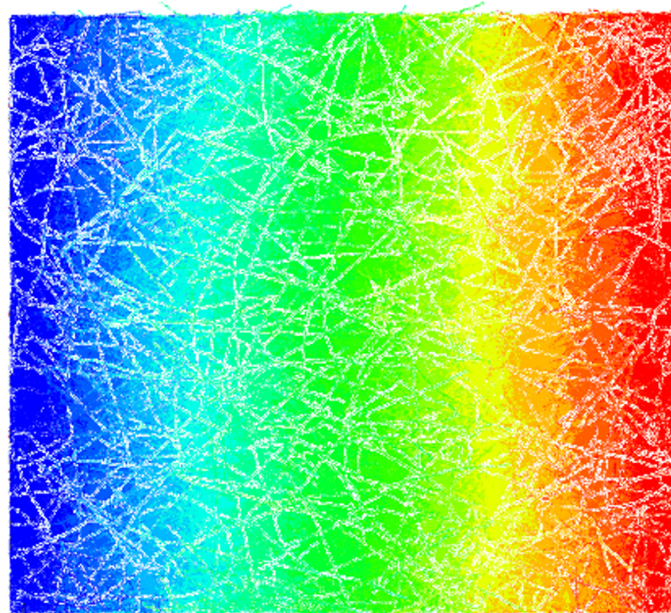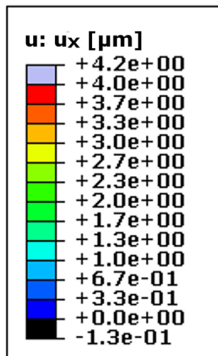
Fig 4. Model A—Deformation plot. Obtained u_x [μm] for sample 316L-20%-No.1 with h_{BC} = 7.75 or 77.50 μm in load case i = 1 (tensile-x).

calculated as follows:

$$Z_{(V_k)} = \frac{1}{n_k} \sum_{j=1}^{j=n_k} Z_{(V_k j)} \tag{12}$$

$$D_{Z(V_k)}^2 = \frac{1}{n_k - 1} \sum_{j=1}^{j=n_k} \left(Z_{(V_k j)} - \overline{Z_{(V_k)}} \right)^2 \tag{13}$$

Using the expressions gained in Eqs (12) and (13), the absolute sampling error ϵ_{abs} and ϵ_{rel} are defined for this algorithm, following [29, 42, 67]:

$$\epsilon_{abs} = \frac{2D_{Z(V)}}{\sqrt{n}} \tag{14}$$

$$\epsilon_{rel} = \frac{\epsilon_{abs}}{Z} \tag{15}$$

V is linked to the variation $D_{Z(V)}^2$ and the point variance D_Z^2 [29, 42, 68]:

$$D_{Z(V)}^2 = D_Z^2 \times \left(\frac{A_3}{V} \right)^\alpha \tag{16}$$

$$D_Z^2 = f(1-f)(Z_{fibre} - Z_{void})^2 \tag{17}$$

Z_{fibre} takes in the present study the value of the respective physical property in V_{fibre}, Z_{void} of the property in V_{void} (with $E_{void} = 0$). Eq (16) requires from the sample volume V [29]:

$$V \gg A_3 \tag{18}$$

The term integral range A_3 [69–72] provides a mathematical measure for the characterisation of random structures.

Inserting Eq (14) into Eq (16) yields Eq (19) which provides for Z the required relation between V, ϵ_{abs}, and n [29, 42]:

$$n = \frac{4}{\epsilon_{abs}^2} D_Z^2 \left(\frac{A_3}{V} \right)^\alpha \tag{19}$$

Eq (19) can be transformed into the final RVE-formula. Now, V stands for the sought variable V_{RVE} [29, 42]:

$$V_{RVE} = \left(\frac{4}{n\,\epsilon_{abs}^2} D_Z^2 A_3^\alpha \right)^{\frac{1}{\alpha}} = \left(\frac{4}{n\,\epsilon_{rel}^2 \overline{Z}^2} D_Z^2 A_3^\alpha \right)^{\frac{1}{\alpha}} \tag{20}$$

In Eq (20), only two unknown variables remain whose values need to be determined for the calculation of V_{RVE}, i.e. A_3 and the exponential RVE-factor α. Linear regression ($y = ax + b$) of

the log-transformed relation given in Eq (16) produces these two values [29, 42]:

$$
\begin{aligned}
log(D^2_{Z(V)}) &= -\alpha\, log(V) + (log(D^2_Z) + \alpha\, log(A_3)) \\
y &:= log(D^2_Z(V)) \\
a &:= -\alpha \\
x &:= log(V) \\
b &:= log(D^2_Z) + \alpha\, log(A_3)
\end{aligned}
\tag{21}
$$

Results and Discussion

FE modelling of experimental in-plane Young's modulus

The transverse Young's modulus $E_T (= \frac{1}{2}(E_x + E_y))$ is obtained through the in-plane load cases $i = 1$ and 2 by Model A and B. The experimental results of [36] are approximated by Model B.

Model A—Rigid joint model. The value of h_{BC} has a non-negligible influence on the obtained E_T in particular for $h_{BC} < 77.50$ μm (see Fig 3 for the exemplary values of sample 316L-10%-No.1, and 316L-20%-No.1). Whether h_{BC} still changes E_T for $h_{BC} \geq 77.50$ μm depends on the imposed BC type. The deformation plots demonstrate for MBC that for low h_{BC} the applied BC cause a mechanical response almost exclusively in the close proximity to the two constrained cube faces F_{x0} and F_{x1} (see Fig 4). For greater h_{BC}, a nearly linear displacement increase through the sample along the axis of tension can be observed in analogy to the increased E_T in Fig 3.

The change from linear to quadratic interpolation decreases the E_T obtained by Timoshenko beams only marginally (see Tables 4 and 5). E_T increases considerably when Euler-Bernoulli beams are simulated:

$$
E_{T,B32} \lesssim E_{T,B31} < E_{T,B33}
\tag{22}
$$

The reduced number of prescribed degrees of freedom (DOF) in the case of MBC reduces also the value of E_T when compared to KUBC:

$$
E_{T,MBC} < E_{T,KUBC}
\tag{23}
$$

The findings in Eqs (22) and (23) hold true irrespectively of the h_{BC} value and confirm the prediction of [62] and [29] respectively.

Model B—Spring joint model. E_T is obtained by Model B for values of s defined in Table 2 with $h_{BC} = 77.50$ μm. This h_{BC} value is chosen because of the obtained E_T magnitude

Table 4. Model A—Influence of beam type on E_T under MBC.

BC: MBC		h_{BC}:				
316L-Sample:	Ratio:	7.75	38.75	77.50	155.00	[μm]
10%-No.1	$E_{T,B33}/E_{T,B31}$	131.05%	137.45%	138.44%	139.62%	[-]
15%-No.1	$E_{T,B33}/E_{T,B31}$	137.63%	143.10%	143.88%	148.88%	
20%-No.1	$E_{T,B33}/E_{T,B31}$	139.45%	142.35%	142.79%	143.53%	
10%-No.1	$E_{T,B32}/E_{T,B31}$	99.44%	99.31%	99.26%	99.27%	[-]
15%-No.1	$E_{T,B32}/E_{T,B31}$	99.12%	99.00%	98.99%	98.99%	
20%-No.1	$E_{T,B32}/E_{T,B31}$	98.65%	98.49%	98.47%	98.47%	

Table 5. Model A—Influence of beam type on E_T under KUBC.

BC: KUBC		h_{BC}:				
316L-Sample:	Ratio:	7.75	38.75	77.50	155.00	[μm]
10%-No.1	$E_{T,\text{B33}}/E_{T,\text{B31}}$	139.02%	153.55%	155.84%	160.58%	[-]
15%-No.1	$E_{T,\text{B33}}/E_{T,\text{B31}}$	147.34%	151.64%	161.01%	168.81%	
20%-No.1	$E_{T,\text{B33}}/E_{T,\text{B31}}$	148.79%	153.94%	154.38%	165.32%	
10%-No.1	$E_{T,\text{B32}}/E_{T,\text{B31}}$	99.34%	99.35%	99.39%	99.50%	[-]
15%-No.1	$E_{T,\text{B32}}/E_{T,\text{B31}}$	99.04%	99.11%	99.21%	99.34%	
20%-No.1	$E_{T,\text{B32}}/E_{T,\text{B31}}$	98.63%	98.77%	98.91%	99.12%	

doi:10.1371/journal.pone.0143011.t005

under MBC (similar to the experimental values of [36]) and because of the considerably reduced dE_T/dh_{BC} at this value. As required, results for Model B tend towards Model A for greater s independently of the applied BC (see Fig 5):

$$\lim_{s[m]\to\infty} E_{T,\text{B}(s)} = E_{T,\text{A}} \tag{24}$$

Under MBC with only two constrained cube faces, E_T results match better the experimentally obtained stiffness values of in-plane tensile testing of [36]. The best match of Model B under MBC is obtained for s = 5 μm (see Fig 6) which is used for the following analyses.

Stiffness matrix and transverse isotropy

The dominantly in-plane fibre orientation of the network samples (see [36, 73] for detailed analyses) influences the mechanical behaviour to a great extent when the remaining load cases i = 3 to 6 (see Fig 7 for sample 316L-20%-No.2) are obtained. It can be described as transversely isotropic.

Eqs (25)–(27) present the elastic moduli together with the confidence intervals $[C_{ij} \pm 2D_{C_{ij}}]$ under KUBC for B32 of each f. All non-bold entries would be expected to equal zero. However, they only nearly vanish which is caused by the numerical artefacts. C_{11} deviates from C_{22} by a maximum error of 6.13% for f = 10%. The conditions that $C_{44} \approx C_{55}$ and $C_{13} \approx C_{23}$ show the biggest errors for f = 15% (5.67% and 4.80% respectively). The obtained error for $C_{66} \approx \frac{1}{2}(C_{11} - C_{12})$ varies between 3.20% for f = 10% and 11.27% for f = 20%.

$$\overline{[C]}_{f=10\%}^{\text{B32}} = \begin{bmatrix} \mathbf{3.25 \pm 0.27} & \mathbf{1.01 \pm 0.06} & \mathbf{0.10 \pm 0.03} & 0.02 \pm 0.03 & 0.06 \pm 0.04 & 0.07 \pm 0.08 \\ \cdot & \mathbf{3.05 \pm 0.09} & \mathbf{0.10 \pm 0.03} & 0.06 \pm 0.08 & 0.03 \pm 0.02 & 0.12 \pm 0.08 \\ \cdot & \cdot & \mathbf{0.32 \pm 0.01} & 0.02 \pm 0.02 & 0.02 \pm 0.03 & 0.02 \pm 0.02 \\ \cdot & \cdot & \cdot & \mathbf{0.17 \pm 0.02} & 0.01 \pm 0.00 & 0.04 \pm 0.04 \\ \cdot & \cdot & \cdot & \cdot & \mathbf{0.17 \pm 0.02} & 0.02 \pm 0.02 \\ \cdot & \cdot & \cdot & \cdot & \cdot & \mathbf{1.09 \pm 0.04} \end{bmatrix} \text{GPa} \tag{25}$$
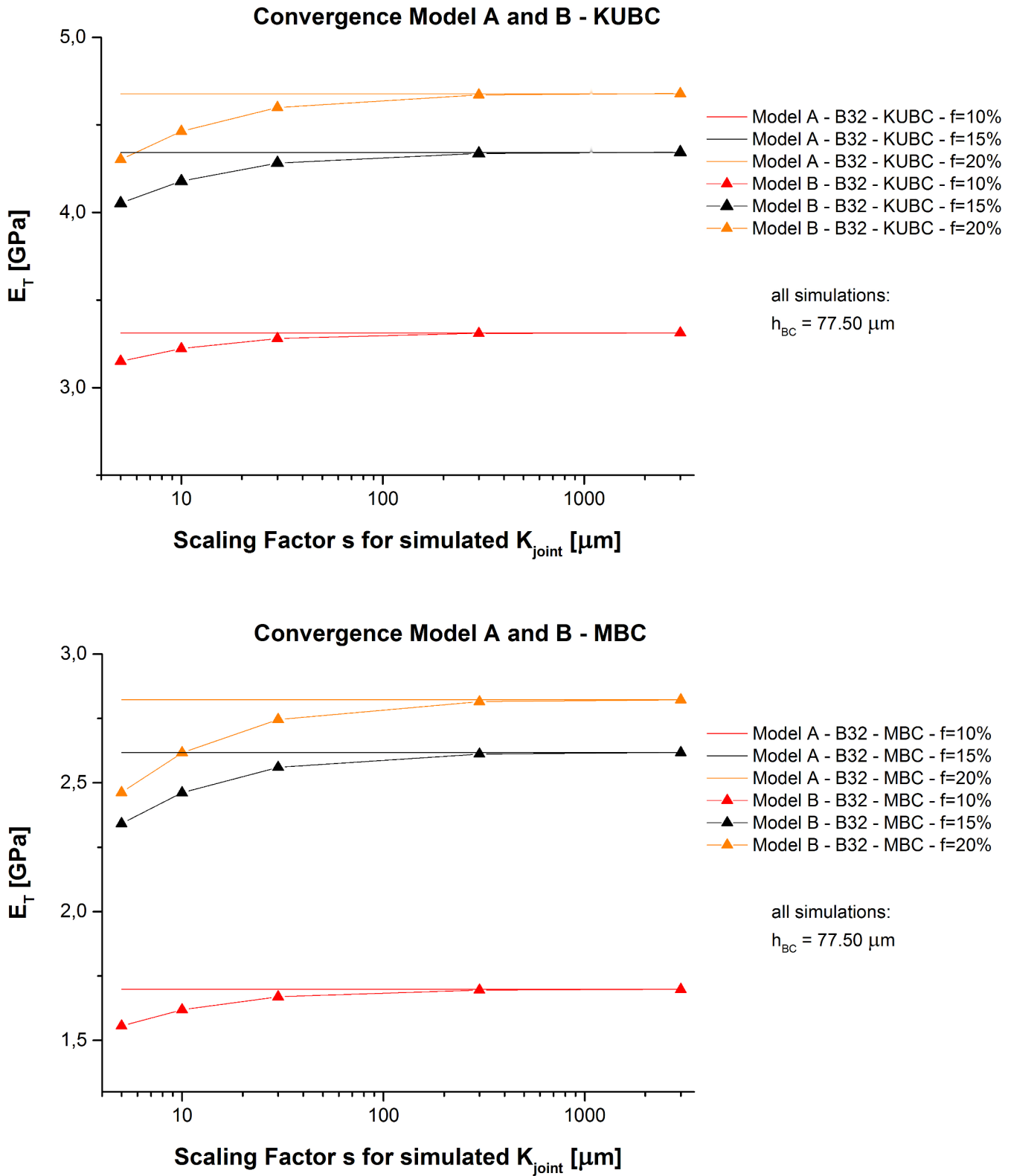
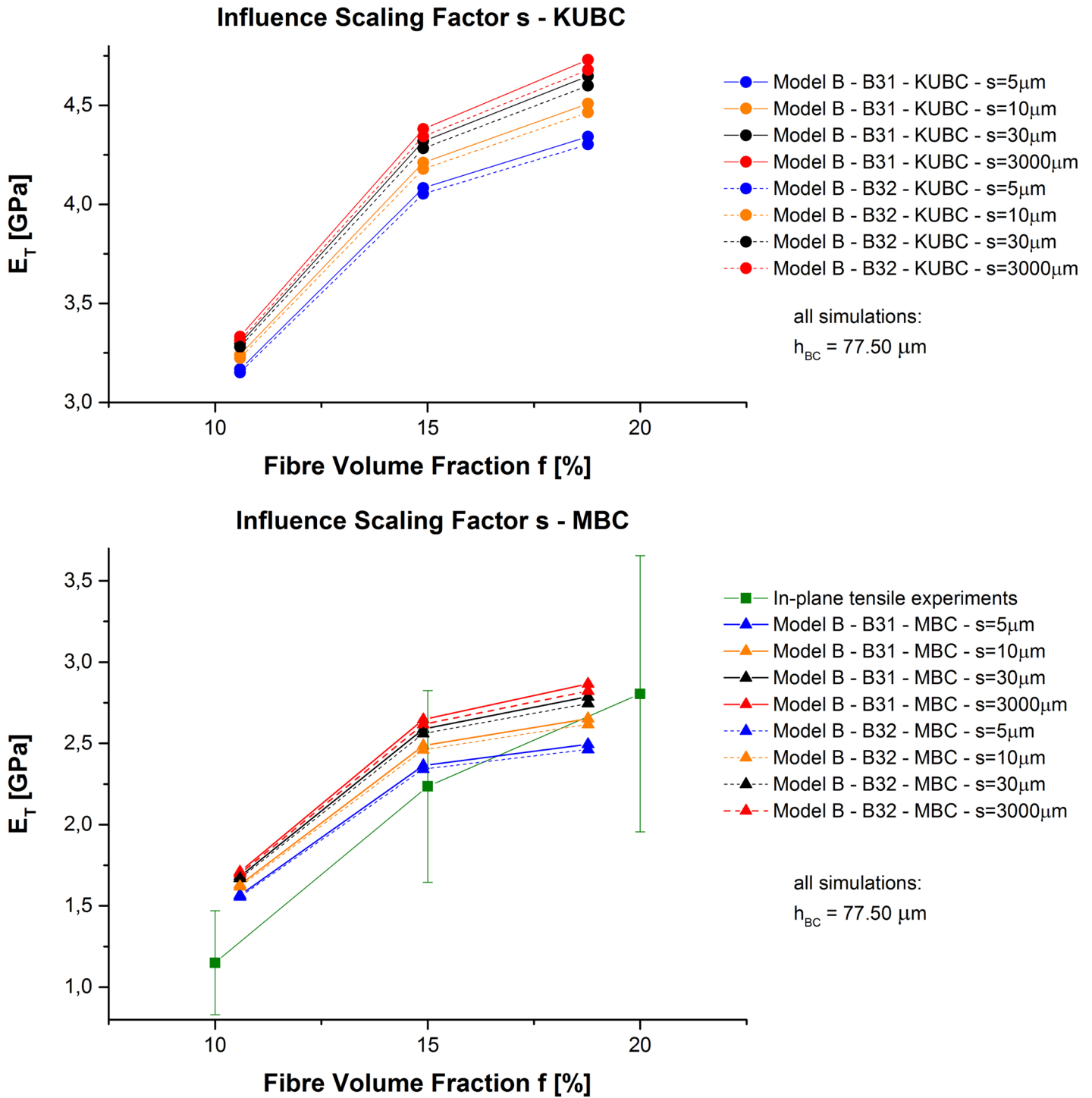Fig 5. Model A and B—Convergence of results. Obtained E_T values of Model A and Model B depending on s.

Fig 6. Model B—Comparison experiments and simulation. Obtained E_T values of Model B depending on f and experimental in-plane tensile testing results of [36].
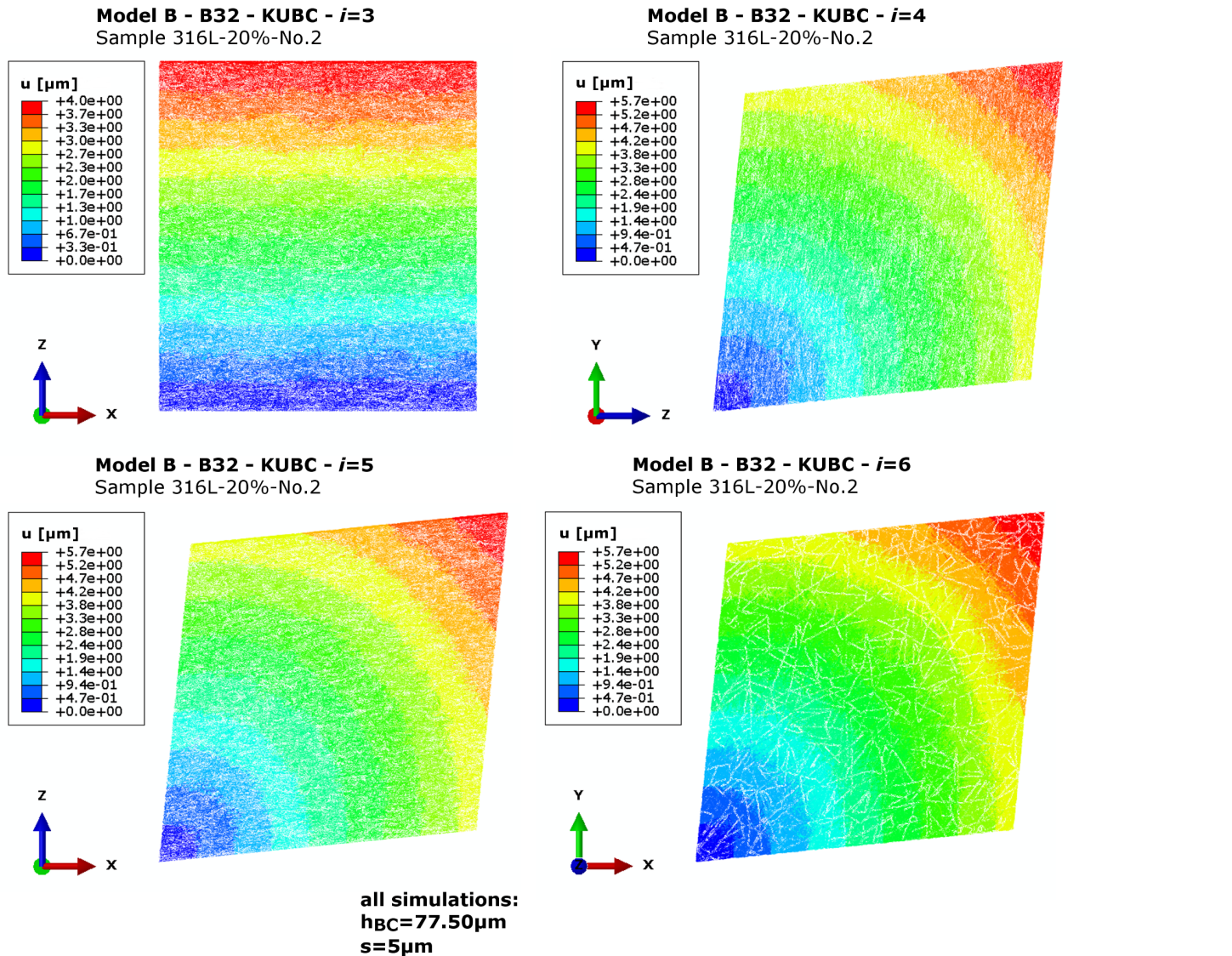
doi:10.1371/journal.pone.0143011.g006

Fig 7. **Model B—Deformation plot.** Obtained u [μm] for sample 316L-20%-No.2 in load cases i = 3 to 6.

doi:10.1371/journal.pone.0143011.g007

$$
\overline{[C]}_{f=15\%}^{B32} = \begin{bmatrix} \mathbf{4.06 \pm 0.07} & \mathbf{1.28 \pm 0.10} & \mathbf{0.18 \pm 0.06} & 0.04 \pm 0.05 & 0.13 \pm 0.21 & 0.11 \pm 0.05 \\ \cdot & \mathbf{4.06 \pm 0.10} & \mathbf{0.17 \pm 0.03} & 0.11 \pm 0.18 & 0.05 \pm 0.05 & 0.13 \pm 0.07 \\ \cdot & \cdot & \mathbf{0.53 \pm 0.09} & 0.04 \pm 0.05 & 0.04 \pm 0.03 & 0.04 \pm 0.02 \\ \cdot & \cdot & \cdot & \mathbf{0.29 \pm 0.01} & 0.02 \pm 0.01 & 0.03 \pm 0.01 \\ \cdot & \cdot & \cdot & \cdot & \mathbf{0.31 \pm 0.05} & 0.03 \pm 0.02 \\ \cdot & \cdot & \cdot & \cdot & \cdot & \mathbf{1.31 \pm 0.12} \end{bmatrix} \text{GPa} \quad (26)
$$

Table 6. Sample set of random realisations for each fibre volume fraction.

Index k	1	2	3	4	5	6	Full sample	
Sub-sample size $V_k^{1/3}$	50	100	150	200	250	300	516	[pixel]
	0.39	0.78	1.16	1.55	1.94	2.33	4.00	[mm]
Number of realisations n_k	140	110	80	50	30	10	2	[-]

doi:10.1371/journal.pone.0143011.t006

$$\overline{[C]}_{f=20\%}^{B32} = \begin{bmatrix} 4.31 \pm 0.14 & 1.32 \pm 0.06 & 0.28 \pm 0.05 & 0.02 \pm 0.01 & 0.05 \pm 0.04 & 0.09 \pm 0.05 \\ \cdot & 4.30 \pm 0.12 & 0.28 \pm 0.04 & 0.06 \pm 0.07 & 0.03 \pm 0.03 & 0.14 \pm 0.26 \\ \cdot & \cdot & 1.02 \pm 0.05 & 0.03 \pm 0.02 & 0.05 \pm 0.07 & 0.04 \pm 0.03 \\ \cdot & \cdot & \cdot & 0.46 \pm 0.05 & 0.02 \pm 0.01 & 0.04 \pm 0.03 \\ \cdot & \cdot & \cdot & \cdot & 0.47 \pm 0.01 & 0.03 \pm 0.03 \\ \cdot & \cdot & \cdot & \cdot & \cdot & 1.33 \pm 0.02 \end{bmatrix} \text{GPa} \quad (27)$$

Size effect and prediction of RVE size

The sample set of V_k and respective n_k in Table 6 with k between 1 and 6 was extracted randomly for each f from the network samples. n_k replicates the scheme found in [45]. The original publication [29] relates to the measurement error which would be rather difficult to quantify for the presented meshed fibres network systems.

E_T shows for the two BC types two different size effects, decreasing for KUBC and increasing for MBC (see Fig 8). These two patterns can be found similarly in [29], there in particular for the bulk modulus under MBC, and for KUBC in [32].

The application of the regression algorithm in Eq (21) (with $Z = E_T$) leads to the values of Table 7. Greater f reduces V_{RVE,E_T}. The influence of the BC type on the material is found to be as predicted by [29]:

$$V_{\mathrm{RVE,MBC}} > V_{\mathrm{RVE,KUBC}} \quad (28)$$

For $f = 10\%$ under MBC, the condition of Eq (18) [29] isn't fulfilled any more. The precision of the values for this particular simulation point could be investigated further in future work by greater sample sets.

Prediction of fibre deformation mechanism

The fibre segment deformation inside the network sample by deflection w^* (perpendicular to the fibre segment axis) is compared to the elongation $\Delta\Lambda$ (along the axis) by the median of their ratio under KUBC (see Fig 9). For greater simplicity, load cases $i = 1$ and 2 are summarised to ϵ_T, $i = 4$ and 5 to the out-of-plane shear deformation $\epsilon_{\mathrm{shear\text{-}z}}$. Load case $i = 3$ stands for $\epsilon_{\mathrm{tensile\text{-}z}}$ and $i = 6$ for $\epsilon_{\mathrm{shear\text{-}xy}}$.

Increased f has been shown to reduce the fibre segment length λ (see Table 1 and [36]) which reduces simultaneously in the present study the obtained median $[w^*/\Delta\Lambda]$. The obtained
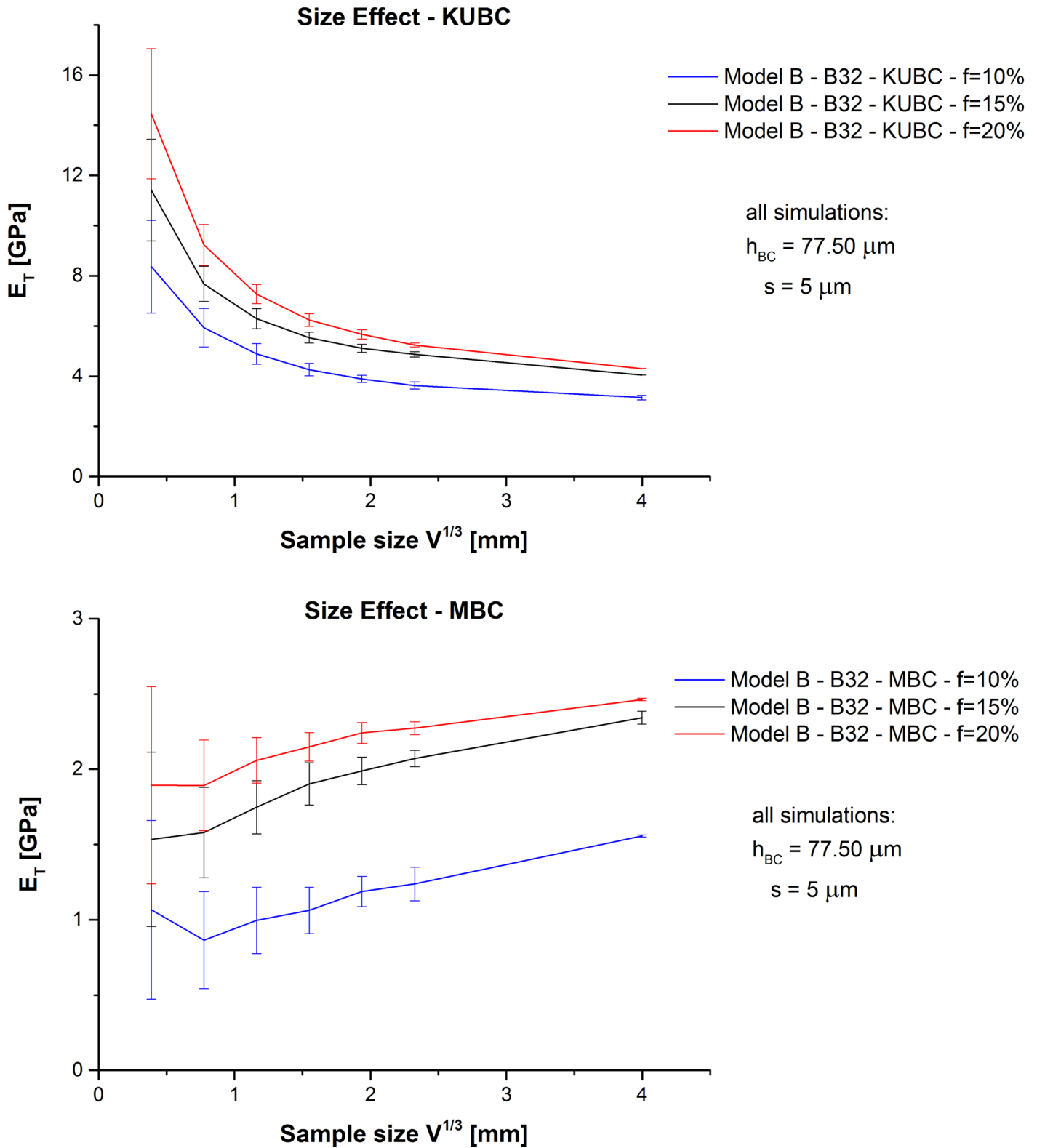
Fig 8. Model B—Size effect. Obtained E_T values of Model B depending on $V^{1/3}$ (error bar = $\pm D_{E_T(V^{1/3})}$).

Table 7. RVE results for KUBC and MBC, obtained by linear regression.

BC -	Values from linear regression			RVE $V_{\mathrm{RVE}.E_T}^{1/3}$ [mm]		
Fibre volume fraction f	α [-]	$A_3^{1/3}$ [mm]	R^2 [-]	$n = 1$, $\epsilon_{rel} = 1\%$	$n = 2$, $\epsilon_{rel} = 1\%$	$n = 5$, $\epsilon_{rel} = 1\%$
KUBC—10%	0.97	0.036	0.97	5.64	4.47	3.29
KUBC—15%	0.90	0.009	0.98	2.25	1.74	1.24
KUBC—20%	0.81	0.003	0.95	1.12	0.84	0.58
MBC—10%	1.41	21.274	0.89	1,210.50	1,042.56	855.84
MBC—15%	1.15	0.294	0.94	39.44	32.62	25.38
MBC—20%	0.94	0.010	0.93	5.06	3.98	2.89

doi:10.1371/journal.pone.0143011.t007

Fig 9. Model B—Deformation mechanism. Obtained median of [$w^*/\Delta\Lambda$] depending on f.

doi:10.1371/journal.pone.0143011.g009

median ratio is in each case greater than 2, increasing for shear and out-of-plane deformation:

$$2 < \left[\frac{w^*}{\Delta\Lambda}\right]^{\mathrm{Median}}_{\epsilon_T} < \left[\frac{w^*}{\Delta\Lambda}\right]^{\mathrm{Median}}_{\epsilon_{shear-xy}} < \left[\frac{w^*}{\Delta\Lambda}\right]^{\mathrm{Median}}_{\epsilon_{tensile-z}} < \left[\frac{w^*}{\Delta\Lambda}\right]^{\mathrm{Median}}_{\epsilon_{shear-z}} < 8 \qquad (29)$$

Conclusions and Future Work

The present study simulates the elastic mechanics of metallic fibre networks by two FE models (rigid inter-fibre joints or torsional spring connectors) and validates the results by experimentally obtained values from [36]. While [29, 32] used solid volume meshes, beam theory is shown to offer a valid simplification method for the investigated material.

BC types MBC and KUBC are simulated and a new model parameter h_{BC} is introduced for the depth to which BC are prescribed into the material along $\underline{n}^{in}$ on ∂V. MBC with fewer prescribed DOF provide a greater match to the experimental values of in-plane tensile testing than KUBC do. The results for rigid inter-fibre joints and for torsional spring connectors converge incrementally. During this process, the influence of the spring constant on the overall

structural stiffness decreases. This implies for the manufacturing process that the stiffness of inter-fibre joints becomes increasingly negligible as soon as a minimum joint strength has been achieved in the sintering process.

In [29], an isotropic material behaviour was obtained for computer generated fibre networks without preferred fibre orientation direction. The material of the present study exhibits a dominantly in-plane fibre orientation [36] and an in-plane transversely isotropic mechanical behaviour. Depending on the applied BC type, a decreasing or increasing size effect is observed. Fibre segment deflection dominates the deformation inside the network over fibre segment elongation. These three findings imply for future work and future design studies that size and shape of the material are of importance, as well as the manufactured fibre orientation.

Of interest for future work is also the achievable strain magnitude in a matrix material located in the network's void phase and the material's suitability for mechanical bone growth stimulation [74].

Acknowledgments

Author Contributions

Conceived and designed the experiments: WAB. Performed the experiments: WAB. Analyzed the data: WAB. Contributed reagents/materials/analysis tools: WAB. Wrote the paper: WAB.

References

1. Ducheyne P, Aernoudt E, De Meester P. The mechanical behaviour of porous austenitic stainless steel fibre structures. Journal of Materials Science. 1978; 13(12):2650–2658. doi: 10.1007/BF02402752

2. Cox H. The elasticity and strength of paper and other fibrous materials. British Journal of Applied Physics. 1951; 3(3):72–79. doi: 10.1088/0508-3443/3/3/302

3. Rigdahl M, Andersson H, Westerlind B, Hollmark H. Elastic Behaviour of Low Density Paper Described by Network Mechanics. Fibre Science and Technology. 1983; 19(2):127–144. doi: 10.1016/0015-0568(83)90036-2

4. Rigdahl M, Westerlind B, Hollmark H. Analysis of cellulose networks by the finite element method. Journal of Materials Science. 1984; 19(12):3945–3952. doi: 10.1007/BF00980758

5. Alava M, Niskanen K. The physics of paper. Reports on Progress in Physics. 2006 mar; 69(3):669–723. doi: 10.1088/0034-4885/69/3/R03

6. Alkhagen M, Toll S. The Effect of Fiber Diameter Distribution on the Elasticity of a Fiber Mass. Journal of Applied Mechanics. 2009; 76(4):041014. doi: 10.1115/1.2966178

7. Head DA, Levine AJ, MacKintosh FC. Mechanical response of semiflexible networks to localized perturbations. Physical Review E. 2005 dec; 72(6):061914. doi: 10.1103/PhysRevE.72.061914

8. Heussinger C, Frey E. Role of architecture in the elastic response of semiflexible polymer and fiber networks. Physical Review E. 2007 jan; 75(1):011917. doi: 10.1103/PhysRevE.75.011917

9. Bai M, Missel AR, Levine AJ, Klug WS. On the role of the filament length distribution in the mechanics of semiflexible networks. Acta biomaterialia. 2011 may; 7(5):2109–2118. doi: 10.1016/j.actbio.2010.12.025 PMID: 21187172

10. Kurniawan NA, Enemark S, Rajagopalan R. The role of structure in the nonlinear mechanics of cross-linked semiflexible polymer networks. The Journal of Chemical Physics. 2012 feb; 136(6):065101. doi: 10.1063/1.3682779 PMID: 22360221

11. Carrillo JMY, MacKintosh FC, Dobrynin AV. Nonlinear Elasticity: From Single Chain to Networks and Gels. Macromolecules. 2013 may; 46(9):3679–3692. doi: 10.1021/ma400478f

12. Mao N, Russell SJ, Pourdeyhimi B. 9 Characterisation, testing and modelling of nonwoven fabrics. In: Russell SJ, editor. Handbook of nonwovens. Cambridge (UK); 2007. p. 401–502.

13. Mannarino MM, Rutledge GC. Mechanical and tribological properties of electrospun PA 6(3)T fiber mats. Polymer. 2012; 53(14):3017–3025. doi: 10.1016/j.polymer.2012.04.039

14. Ridruejo A, González C, LLorca J. A constitutive model for the in-plane mechanical behavior of nonwoven fabrics. International Journal of Solids and Structures. 2012 sep; 49(17):2215–2229. doi: 10.1016/j.ijsolstr.2012.04.014

15. Silberstein MN, Pai CL, Rutledge GC, Boyce MC. Elastic-plastic behavior of non-woven fibrous mats. Journal of the Mechanics and Physics of Solids. 2012 feb; 60(2):295–318. doi: 10.1016/j.jmps.2011.10.007

16. Farukh F, Demirci E, Sabuncuoglu B, Acar M, Pourdeyhimi B, Silberschmidt VV. Numerical analysis of progressive damage in nonwoven fibrous networks under tension. International Journal of Solids and Structures. 2014; 51(9):1670–1685. doi: 10.1016/j.ijsolstr.2014.01.015

17. Farukh F, Demirci E, Sabuncuoglu B, Acar M, Pourdeyhimi B, Silberschmidt VV. Mechanical analysis of bi-component-fibre nonwovens: Finite-element strategy. Composites Part B: Engineering. 2015; 68:327–335. doi: 10.1016/j.compositesb.2014.09.003

18. Kwon RY, Lew AJ, Jacobs CR. A microstructurally informed model for the mechanical response of three-dimensional actin networks. Computer Methods in Biomechanics and Biomedical Engineering. 2008 aug; 11(4):407–418. doi: 10.1080/10255840801888686 PMID: 18568835

19. Lieleg O, Schmoller KM, Claessens MMAE, Bausch AR. Cytoskeletal polymer networks: viscoelastic properties are determined by the microscopic interaction potential of cross-links. Biophysical journal. 2009 jun; 96(11):4725–4732. doi: 10.1016/j.bpj.2009.03.038 PMID: 19486695

20. Fletcher DA, Mullins RD. Cell mechanics and the cytoskeleton. Nature. 2010 jan; 463(7280):485–492. doi: 10.1038/nature08908 PMID: 20110992

21. Stricker J, Falzone T, Gardel ML. Mechanics of the F-actin cytoskeleton. Journal of Biomechanics. 2010 jan; 43(1):9–14. doi: 10.1016/j.jbiomech.2009.09.003 PMID: 19913792

22. Yamaoka H, Matsushita S, Shimada Y, Adachi T. Multiscale modeling and mechanics of filamentous actin cytoskeleton. Biomechanics and modeling in mechanobiology. 2012 mar; 11(3):291–302. doi: 10.1007/s10237-011-0317-z PMID: 21614531

23. Astrom JA, Makinen JP, Hirvonen H, Timonen J. Stiffness of compressed fiber mats. Journal of Applied Physics. 2000; 88(9):5056–5061. doi: 10.1063/1.1315622

24. Head DA, MacKintosh FC, Levine AJ. Nonuniversality of elastic exponents in random bond-bending networks. Physical Review E. 2003 aug; 68(2):025101(R). doi: 10.1103/PhysRevE.68.025101

25. DiDonna BA, Lubensky TC. Nonaffine correlations in random elastic media. Physical Review E. 2005 dec; 72(6):066619. doi: 10.1103/PhysRevE.72.066619

26. Hatami-Marbini H, Picu RC. Heterogeneous long-range correlated deformation of semiflexible random fiber networks. Physical Review E. 2009 oct; 80(4):046703. doi: 10.1103/PhysRevE.80.046703

27. Broedersz CP, Sheinman M, MacKintosh FC. Filament-Length-Controlled Elasticity in 3D Fiber Networks. Physical Review Letters. 2012 feb; 108(7):078102. doi: 10.1103/PhysRevLett.108.078102 PMID: 22401259

28. Shahsavari AS, Picu RC. Size effect on mechanical behavior of random fiber networks. International Journal of Solids and Structures. 2013 oct; 50(20-21):3332–3338. doi: 10.1016/j.ijsolstr.2013.06.004

29. Dirrenberger J, Forest S, Jeulin D. Towards gigantic RVE sizes for 3D stochastic fibrous networks. International Journal of Solids and Structures. 2014 jan; 51(2):359–376. doi: 10.1016/j.ijsolstr.2013.10.011

30. Jin MZ, Chen CQ, Lu TJ. The mechanical behavior of porous metal fiber sintered sheets. Journal of the Mechanics and Physics of Solids. 2013 jan; 61(1):161–174. doi: 10.1016/j.jmps.2012.08.006

31. Zhao TF, Jin MZ, Chen CQ. A phenomenological elastoplastic model for porous metal fiber sintered sheets. Materials Science and Engineering: A. 2013 oct; 582:188–193. doi: 10.1016/j.msea.2013.06.042

32. Tsarouchas D. Fibre Network Materials: Architecture & Effective Linear Elastic Properties. University of Cambridge; 2012.

33. Yi P, Peng L, Liu N, Lai X, Ni J. A micromechanics elastic-plastic constitutive model for sintered stainless steel fiber felt. Materials & Design. 2013 oct; 51:876–885. doi: 10.1016/j.matdes.2013.05.023

34. Rodney D, Gadot B, Martinez OR, du Roscoat SR, Orgéas L. Reversible dilatancy in entangled single-wire materials. Nature Materials. 2015;(September (advance online publication)). Available from: http://www.nature.com/doifinder/10.1038/nmat4429

35. Bosbach W. The mechanical and magnetic behaviour of sintered fibre networks and their suitability for a therapeutic, biomedical application. University of Cambridge (viva passed on 20 March 2015); 2015.

36. Neelakantan S, Bosbach W, Woodhouse J, Markaki AE. Characterization and deformation response of orthotropic fibre networks with auxetic out-of-plane behaviour. Acta Materialia. 2014 mar; 66:326–339. doi: 10.1016/j.actamat.2013.11.020

37. Wieding J, Souffrant R, Fritsche A, Mittelmeier W, Bader R. Finite Element Analysis of Osteosynthesis Screw Fixation in the Bone Stock: An Appropriate Method for Automatic Screw Modelling. PloS ONE. 2012 jan; 7(3):1–10. doi: 10.1371/journal.pone.0033776

38. Eulero L. Methodus inveniendi lineas curvas maximi minimive proprietate gaudentes, sive solutio problematis isoperimetrici latissimo sensu accepti. Lausanne (Switzerland); 1744.

39. Timoshenko S. On the Correction for Shear of the Differential Equation for Transverse Vibrations of Prismatic Bars. Philosophical Magazine Series 6. 1921; 41(245):744–746. doi: 10.1080/14786442108636264

40. Timoshenko S. On the transverse vibrations of bars of uniform cross-section. Philosophical Magazine Series 6. 1922; 43(253):125–131. doi: 10.1080/14786442208633855

41. Reddy JN. An Introduction to the Finite Element Method. 3rd ed. College Station, Texas (USA); 2006.

42. Kanit T, Forest S, Galliet I, Mounoury V, Jeulin D. Determination of the size of the representative volume element for random composites: statistical and numerical approach. International Journal of Solids and Structures. 2003 jun; 40(13-14):3647–3679. doi: 10.1016/S0020-7683(03)00143-4

43. Kanit T, N'Guyen F, Forest S, Jeulin D, Reed M, Singleton S. Apparent and effective physical properties of heterogeneous materials: Representativity of samples of two materials from food industry. Computer Methods in Applied Mechanics and Engineering. 2006 jul; 195(33-36):3960–3982. doi: 10.1016/j.cma.2005.07.022

44. Brun E, Vicente J, Topin F, Occelli R, Clifton MJ. Microstructure and Transport Properties of Cellular Materials: Representative Volume Element. Advanced Engineering Materials. 2009 oct; 11(10):805–810. doi: 10.1002/adem.200900131

45. Grimal Q, Raum K, Gerisch A, Laugier P. A determination of the minimum sizes of representative volume elements for the prediction of cortical bone elastic properties. Biomechanics and modeling in mechanobiology. 2011 dec; 10(6):925–937. doi: 10.1007/s10237-010-0284-9 PMID: 21267625

46. Kanit T, Forest S, Jeulin D, N'Guyen F, Singleton S. Virtual improvement of ice cream properties by computational homogenization of microstructures. Mechanics Research Communications. 2011 mar; 38(2):136–140. doi: 10.1016/j.mechrescom.2011.01.005

47. Röntgen WC. Ueber eine neue Art von Strahlen (Vorläufige Mittheilung). In: Sonderabbdruck der Sitzungsberichte der Würzburger Physik.-medic. Gesellschaft. Würzburg (Germany); 1895.

48. Buzug M. Computed Tomography—From Photon Statistics to Modern Cone-Beam CT. Luebeck (Germany); 2008.

49. Francois R. US-Patent 5,071,713; 1991.

50. Lee TC, Kashyap RL, Chong-Nam C. Building Skeleton Models via 3-D Medial Surface/Axis Thinning Algorithms. Graphical Models and Image Processing. 1994; 56(6):462–478. doi: 10.1006/cgip.1994.1042

51. Lindquist WB. 3DMA General Users Manual. Stony Brook (USA); 1999.

52. Yang H. A Geometric and Statistical Analysis of Fibrous Materials from Three-Dimensional High Resolution Images. State University of New York at Stony Brook; 2001.

53. Desai CS, Abel JF. Introduction to the Finite Element Method—A Numerical Method for Engineering Analysis. New York (USA); 1972.

54. Hooke R. Lectures de Potentia Restitutiva, or of Spring—Explaining the Power of Springing Bodies. London (UK); 1678.

55. Dassault Systèmes. Abaqus 6.13 Online Documentation; 2013. Available from: http://129.97.46.200:2080/v6.13/

56. Dassault Systèmes. Abaqus Theory Guide 1.5.1 Equilibrium and virtual work; 2013. Available from: http://129.97.46.200:2080/v6.13/books/stm/default.htm?startat = ch01s05ath08.html

57. Logan JD. Applied Mathematics. 6th ed. Lincoln, Nebraska (USA); 2006.

58. Atzberger PJ. Stochastic Eulerian Lagrangian methods for fluid-structure interactions with thermal fluctuations. Journal of Computational Physics. 2011; 230(8):2821–2837. doi: 10.1016/j.jcp.2010.12.028

59. Gross D, Hauger W, Schröder J, Wall WA, Bonet J. Engineering Mechanics 2: Mechanics of Materials. Heidelberg (Germany); 2011.

60. Shahsavari A, Picu RC. Model selection for athermal cross-linked fiber networks. Physical Review E. 2012 jul; 86(1):011923. doi: 10.1103/PhysRevE.86.011923

61. Dassault Systèmes. Abaqus Analysis User's Guide 29.3.3 Choosing a beam element; 2013. Available from: http://129.97.46.200:2080/v6.13/books/usb/default.htm?startat = pt06ch29s03alm08.html

62. Wang CW, Berhan L, Sastry AM. Structure, Mechanics and Failure of Stochastic Fibrous Networks—Part I Microscale Considerations. Journal of Engineering Materials and Technology. 2000; 122(4):450–459. doi: 10.1115/1.1288769

63. Berhan L, Yi YB, Sastry AM, Munoz E, Selvidge M, Baughman R. Mechanical properties of nanotube sheets: Alterations in joint morphology and achievable moduli in manufacturable materials. Journal of Applied Physics. 2004; 95(8):4335–4345. doi: 10.1063/1.1687995

64. Kaw AK. Mechanics of Composite Materials. 2nd ed. Boca Raton, Florida (USA); 2006.

65. Zohdi TI, Wriggers P. An Introduction to Computational Micromechanics. In: Pfeiffer F, Wriggers P, editors. Lecture Notes in Applied and Computational Mechanics. 1st ed. Hannover (Germany); 2005.

66. Christensen RM. 1.1 Elasticity Theory Results. In: Mechanics of Composite Materials. revised ed. Mineola, New York (USA); 2005.

67. Matheron G. Estimating and Choosing. Paris (France); 1989.

68. Jeulin D. Variance scaling of Boolean random varieties. HAL: hal-00618967, version 1. 2011;p. 1–16.

69. Matheron G. The Theory of Regionalized Variables and its Applications. In: Les Cahiers du Centre de Morphologie Mathematique de Fontainebleau. vol. 5. Paris (France); 1971. p. 1–211.

70. Matheron G. Random Sets and Integral Geometry. Paris (France); 1975.

71. Lantuejoul C. Ergodicity and integral range. Journal of Microscopy. 1991; 161(3):387–403. doi: 10.1111/j.1365-2818.1991.tb03099.x

72. Cailletaud G, Jeulin D, Rolland P. Size Effect on Elastic Properties of Random Composites. Engineering Computations. 1994; 11(2):99–110. doi: 10.1108/02644409410799227

73. Spear RL, Srigengan B, Neelakantan S, Bosbach W, Brooks RA, Markaki AE. Physical and Biological Characterization of Ferromagnetic Fiber Networks: Effect of Fibrin Deposition on Short-Term In Vitro Responses of Human Osteoblasts. Tissue Engineering Part A. 2015; 21(3-4):463–474. doi: 10.1089/ten.tea.2014.0211 PMID: 25145466

74. Bosbach W. Finite element modelling of bone growth stimulation and its suitability for therapeutic, biomedical applications. In: von-Behring-Röntgen-Symposium. Giessen (Germany); 2015. p. 1–2. Available from: https://www.repository.cam.ac.uk/handle/1810/251137?show = full